The International Journal of Advanced Manufacturing Technology (2020) 111:1277–1290
https://doi.org/10.1007/s00170-020-06170-4

ORIGINAL ARTICLE

# Burr formation and surface roughness characteristics in micro-milling of microchannels

Liang Chen[1] · Daxiang Deng[2] · Guang Pi[1] · Xiang Huang[3] · Wei Zhou[1]

Received: 22 March 2020 / Accepted: 24 September 2020 / Published online: 9 October 2020


**Abstract**
Microchannels are attractive for their widespread applications in electronics, biological, chemical, and energy areas. Micro-milling provides an ideal method to fabricate microchannels, whereas problematic burr formations and inherent rough surfaces of microchannel bottom and sidewalls are still far from sufficiently known. In this study, micro-milling process of rectangular copper microchannels was conducted by a two-flute tungsten carbide micro-end mill. Burr formation mechanism was studied via 3D finite element simulation together with experiment observations. Surface quality of microchannels, i.e., burr size and surface roughness, was studied in different spindle speeds, feed rates, and depths of cut. It was found that the top burr sizes on the down-milling side of microchannels were much larger than those on the up-milling side. The top burr size on the down-milling side and surface roughness on bottom and both sidewalls of microchannels presented a monotonic decreasing trend when the spindle speed increased, and an increasing trend with increasing depth of cut. Nevertheless, they firstly decreased due to the plowing and extruding effect together with elastic recovery when the feed rate was smaller than the tool cutting edge radius, and then changed to increase due to the shearing and cutting process after the feed rate exceed the tool cutting edge radius. High spindle speed, small depth of cut, and moderate feed rate close to the tool cutting edge radius seem to be favorable to improve surface quality of micro-milled microchannels.

**Keywords** Microchannels · Micro-milling · Burr · Surface roughness

## 1 Introduction

Microchannels have been widely recognized to be an ideal integral component for their widespread applications in microchannel heat exchanger, micro-biochips, micro-reactors, and micro-fuel cells in electronics, biological, chemical, and energy areas [1, 2] since 1981 by Tuckerman and Pease [3]. By controlling, delivering, manipulating, and storing fluid within a miniature area, microchannels feature many promising advantages, such as large heat transfer surface area, excellent heat transfer capacities, compact dimensions, and effectiveness in flow distribution and controlled pressure drop. Therefore, lots of research efforts have been devoted to developing microchannels employing different fabrication methods, such as etching [4], photolithography [5], wire electrical discharge machining (EDM) [6], and laser ablation process [7]. Nevertheless, the etching and photolithography methods are limited to silicon and polymer materials. The EDM and laser ablation methods generally produced microchannels with large errors of geometric dimensions and poor surface qualities. Moreover, the above fabrication methods are somewhat time-consuming and costly [8, 9].

Micro-milling, as one of micro-machining technologies, may be a good choice to fabricate microchannels. Micro-milling is able to produce micro-products of complex shapes with few material restrictions. It can fabricate microstructures with high precision and efficiency, and low cost [10]. To date, the micro-milling has been developed to fabricate microchannels in several reports. Vázquez et al. [11] prepared rectangular microchannels in aluminum alloy and with hardness of 21 HRB and copper alloy with hardness of 72 HRB by

✉ Daxiang Deng
dengdaxiang@hit.edu.cn

[1] Department of Mechanical & Electrical Engineering, Xiamen University, Xiamen 361005, China

[2] School of Mechanical Engineering and Automation, Harbin Institute of Technology, Shenzhen, Shenzhen 518055, China

[3] School of Mechanical Engineering, Zhejiang University of Technology, Hangzhou 310014, China

micro-milling process. The microchannel dimensions, shapes, and surface roughness of microchannel bottom wall have been examined. Results indicated that the use of coolant lubrication in micro-milling helps to improve the achieved dimensions and surface finish of microchannels. The microchannels fabricated in aluminum were of better quality than those in copper. In later studies, Vázquez et al. [12] fabricated arrays of microchannels in aluminum and titanium plates, and explored the multi-criteria decision making for material and processing parameter selection for desired accuracy using particle swarm optimization (PSO) method. Kiswanto et al. [13] fabricated microchannels in Aluminum Alloy AA1100 using flat end mill tools with two flutes of a diameter of 0.2 mm. Using a statistical method ANOVA, it was found that the feed rate and machining time contributed significantly to the surface roughness of the microchannel bottom wall. Lower feed rate would produce better surface roughness in general. Tool wears due to machining time were the most influential factor on burr formation. Wang et al. [14] developed Ti(C7N3)-based cermet micro-mills to mill micro-grooves in TC4 alloy. By the comparison of commercial CrTiAlN-coated WC micro-mills, the cermet micro-mills were found to decrease the cutting forces and burr formation, and improved the tool wear performance. The surface quality of the micro-grooves bottom wall surface was also measured and evaluated. Recently, Han et al. [15] fabricated high aspect ratio micro-grooves with the large length-diameter ratio micro-end mills. The effects of cutting fluids and tool wear of on micro-burr generation and surface quality of the groove bottom wall were analyzed. Results showed that the burr generation and surface quality were strongly dependent on the tool wear and groove depth.

In micro-milling process, the material removal process is strongly dominated by the size effect in micro-milling. The plowing and rubbing process increase the surface roughness and induce remarkable burr formations along the cutting path. Therefore, surface roughness and burr formation are usually utilized as assessment for the selection of micro-milling parameters [13, 15]. A number of researches have been conducted to explore the surface quality and burr generations in micro-milling process. Wang et al. [16] found that the feed rate was the most dominant parameter when other parameters were constant for the micro-milling of brass surface, and surface roughness increased linearly as the tool diameter and spindle speed increased. Jin et al. [17] studied the interaction effect of parameters to surface topography and cutting forces in the micro-milling of AISI D2 steel. Large burr size and surface roughness were induced at a low ratio of feed per tooth to cutting edge radius ratio. Biermann and Kahnis [18] explored the influences of a downscaling of the tool diameter and machining parameters on specific cutting forces, surface roughness, and burr formation in the micro-milling of steel. They found that an enlargement of cutting edge radius contributed to a lower surface quality and a less tool wear. Özel et al. [19] studied the influence of process parameters on surface roughness and burr formation in micro-milling of Ti–6Al–4V alloy by both experiments and FEM simulations. The optimum parameters were determined to minimize both surface roughness and burr formation concurrently. Lekkala et al. [20] performed a comprehensive study on the effect of spindle speed, feed rate, tool diameter, depth of cut, and number of flutes on burr formation in micro-end milling. Results indicated that the depth of cut and the tool diameter are the main parameters for the burr formation, whereas the speed and feed rate show small to negligible effects on the burr generation. Wu et al. [21] found that burr formation decreased to the minimum value when the uncut chip thickness reduced to equal the cutting edge radius, and then increased with further reduction of the uncut chip thickness in the micro-milling of snake-shaped groove microstructure. Gao et al. [22] studied the effects of spindle speed, feed rate, and milling depth on surface roughness in the micro-milling of nickel-based single-crystal superalloy DD98 using the response surface method of central composite design. The feed rate was found to play the most significant role on surface roughness, followed by spindle speed and milling depth.

From the above literature review, it can be noted that many studies have been conducted to explore the surface quality and burr formation in micro-milling process. Nevertheless, the information of micro-milling of microchannels and cutting parameter effects on surface quality and burr formation are far from sufficient. Besides, most of previous studies focus on surface roughness of the bottom wall surfaces after micro-milling, whereas the surface roughness on the sidewall of microchannels is seldom reported. To this end, we in this study comprehensively studied the micro-milling process of microchannels by experiments and simulations. The effects of spindle speed, feed rate, and depth of cut on the burr formations along the microchannels and surface roughness of microchannel bottom and sidewalls were assessed and discussed in detail.

## 2 Experiment

### 2.1 Micro-milling experiments

The micro-milling process of microchannels is performed in a precision CNC engraving and milling machine in wet conditions with conventional emulsion. It equips with a stepper motor with 1 μm motion resolution and 5 μm positioning accuracy for each axis. Three linear axes (X,Y,Z) are used for the manufacturing process. The stroke of each linear axis (X,Y,Z) of the machine is 400 mm, 400 mm, and 200 mm, respectively. The schematic of micro-milling process of microchannels is shown in Fig. 1a. Commercial pure red copper plates (99.9% Cu) with a dimension of 10 mm × 10 mm ×

4 mm are utilized as the workpiece. Two-flute tungsten carbide end mill with a diameter of 0.5 mm is employed as the micro-cutter, as carbide tools are suitable for cutting pure red copper because of their superior abrasion resistance and ability to perform a high speed cutting. Figure 1b and c shows the microscopic images of the micro-milling cutter. Table 1 shows the parameters of the micro-milling cutter.

Before the micro-milling experiments, a pre-cut was launched by a 5-mm milling cutter to ensure the flatness of the workpiece. Parametric experiments were conducted to investigate the effects of processing parameters, i.e., spindle speed, feed rate, and depth of cut, on the burr formation along the microchannels and surface roughness of both bottom and sidewalls of microchannels. As shown in Table 2, the spindle speed varies from 9000 to 21,000 r/min, the feed rate changes from 30 to 150 mm/min which corresponds to 1 μm/z to 5 μm/z (feed per tooth, $f_z$), and the depth of cut varies between 40 and 80 μm.

**Table 1** Parameters of the micro-milling cutter

| Cutter parameter | Value |
|---|---|
| Diameter, $d$ (mm) | 0.5 |
| Cutting edge radius, $r_e$ (μm) | 2 |
| Helix angle, $\beta$ (°) | 35 |
| Rake angle, $\gamma_n$ (°) | 5 |
| Clearance angle, $\alpha_0$ (°) | 12 |

## 2.2 Measurement of surface roughness and burr size of microchannels

After the microchannels are fabricated, the samples are ultrasonically cleaned in ethanol firstly to remove any residues or contaminants on microchannels. The surface morphology and profiles of microchannels are measured by a scanning electron microscope (SEM, HITACHI SU-70) and a 3D Laser Scanning Confocal Microscope (LSM, VK-X200, KEYENCE). The surface roughness of the microchannel bottom and sidewall (both up-milling and down-milling sides) surfaces can be determined by the 3D laser scanning confocal microscope. For the measurement of surface roughness of microchannel sidewall surfaces, the microchannels were cut off from the back side into two sub-parts using wire electrical discharge machining method with a molybdenum electrode with diameter of 50 μm. A typical measurement of the microchannel bottom surface by is illustrated in the Fig. 2. Five randomly chosen areas in parallel microchannels are utilized for the measurement of surface roughness, and the averaged values are taken as the results.

In this study, the top burr width of microchannels is used to evaluate the burr size, which has been adopted by many studies [13, 23, 24]. The total burr width ($W$) is the horizontal distance between the root of the sidewall and the point of burr side. The burr width is measured using SEM, as shown in Fig. 3b. To obtain the burr size, four microchannels were randomly chosen for each sample, and five measurements of burr width in different areas for each microchannel were recorded. The average value of the total 20 measurements was calculated for the final result of burr size of the sample. The burr width on the up-milling side ($W_u$) and down-milling side ($W_d$) were both determined and taken into consideration, as shown in Fig. 3a.

## 2.3 Model establishment of micro-milling of microchannels

In order to explore the burr formation in micro-milling of microchannels, a finite element (FE) simulation of the burr formation process is conducted using a commercial software DEFORM-3D (Code v10.2). Both workpiece and tool models are defined by tetrahedral meshes, and the meshes in the cutting zone and cutting edges are generated using an adaptively remeshing technique with a local mesh refinement size of 1 μm. An updated Lagrangian solution for viscoplastic metal

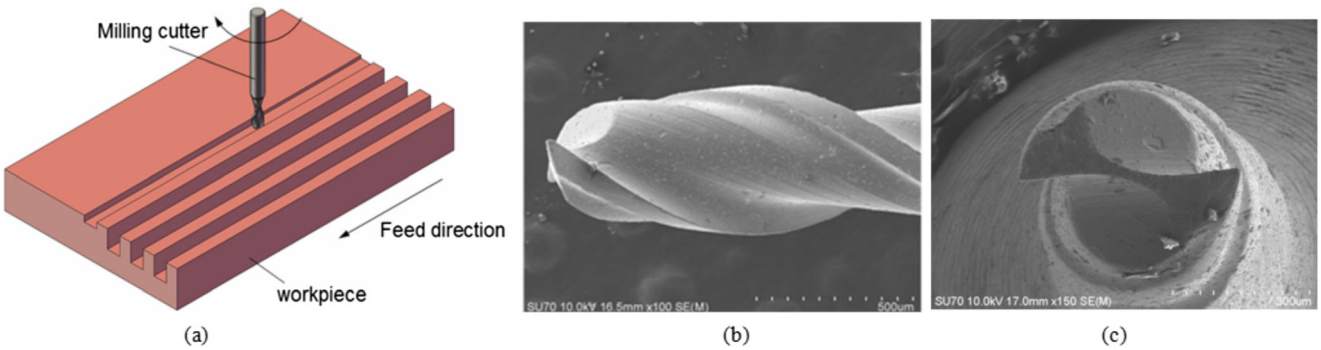


**Fig. 1** **a** Schematic of micro-milling process of microchannels. **b** Top view of SEM images of the micro-milling cutter. **c** Cross-sectional view of SEM images of the cutter

**Table 2** Detail of design of experiments

| No. of exp | Spindle speed (r/min) | Feed rate (mm/min) | Depth of cut (μm) |
|---|---|---|---|
| 1 | 9000 | 90 | 80 |
| 2 | 12,000 | 90 | 80 |
| 3[a] | 15,000 | 90 | 80 |
| 4 | 18,000 | 90 | 80 |
| 5 | 21,000 | 90 | 80 |
| 6 | 15,000 | 30 | 80 |
| 7 | 15,000 | 60 | 80 |
| 8[a] | 15,000 | 90 | 80 |
| 9 | 15,000 | 120 | 80 |
| 10 | 15,000 | 150 | 80 |
| 11 | 15,000 | 90 | 40 |
| 12 | 15,000 | 90 | 60 |
| 13[a] | 15,000 | 90 | 80 |
| 14 | 15,000 | 90 | 100 |
| 15 | 15,000 | 90 | 120 |

[a] The same sample

deformations is utilized in the simulations. Simulation model of the micro-milling process together with the boundary conditions is simplified and shown in Fig. 4. The workpiece is fixed in three directions, and the cutter rotates and feeds in the cutting direction. The dimensions of the workpiece are 4 × 1.5 × 1.5 $mm^3$. The two-flute micro-end mill with Tungsten carbide is used, and is regarded as a rigid body. The diameter of the micro-end mill is 0.5 mm, which is identical to that in the experiments. The parameters of copper material and tungsten carbide micro-end mills are given in Tables 3 and 4, respectively. The geometry model of micro-end mill is established by 3D CAD/CAM software of Solidworks. The cutting surface of the workpiece and the whole surface of the tool are defined as the heat transfer surface, as shown in Fig. 4. The environment temperature is set to be 20 °C. In this study, the shear friction model based on constant shear hypothesis is employed, and the friction factor is assumed to be 0.6.

To properly describe the mechanical behavior of pure copper, a widely used constitutive model in machining simulation proposed by Johnson and Cook (J-C) [25] is used as follows

$$\overline{\sigma} = \left[A + B\left(\overline{\varepsilon}\right)^{n}\right]\left[1 + C\ln\left(\frac{\dot{\overline{\varepsilon}}}{\dot{\overline{\varepsilon}}_0}\right)\right]\left[1-\left(\frac{T-T_{room}}{T_{melt}-T_{room}}\right)^{m}\right] \tag{1}$$

The components in right side of Eq. (1) represent the effects of material strain hardening, strain rate hardening, and thermal softening, respectively. $\overline{\sigma}$ is the equivalent flow stress, $\overline{\varepsilon}$ is the equivalent plastic strain, $\dot{\overline{\varepsilon}}$ is the equivalent plastic strain rate, $\dot{\overline{\varepsilon}}_0$ is the reference equivalent plastic strain, $T$ is the work piece temperature, and $T_{melt}$ and $T_{room}$ are the material melting temperature and room temperature, respectively. The parameters of copper material, tungsten carbide micro-end mills, and parameters in the J-C model are given in Table 5.

## 3 Results and discussion

### 3.1 Burr formation and burr size

#### 3.1.1 Burr formation analysis

The burr formation in micro-milling process was explored by both 3D finite element simulation and experiment observations. According to the forming positions, they are classified into entrance burr, top burr (both on the down-milling side and

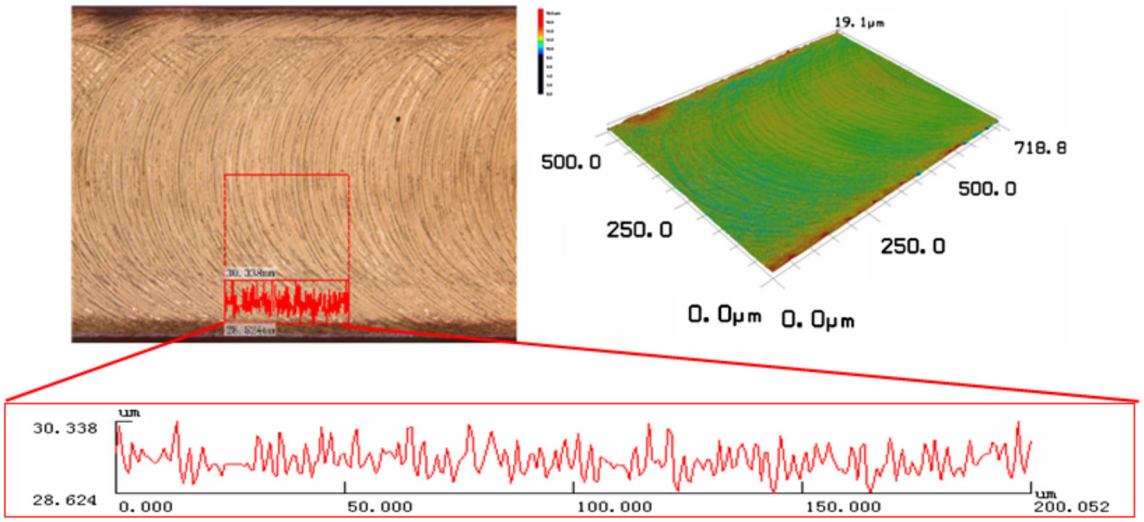


**Fig. 2** Illustration of the roughness measurement by 3D laser scanning confocal microscope

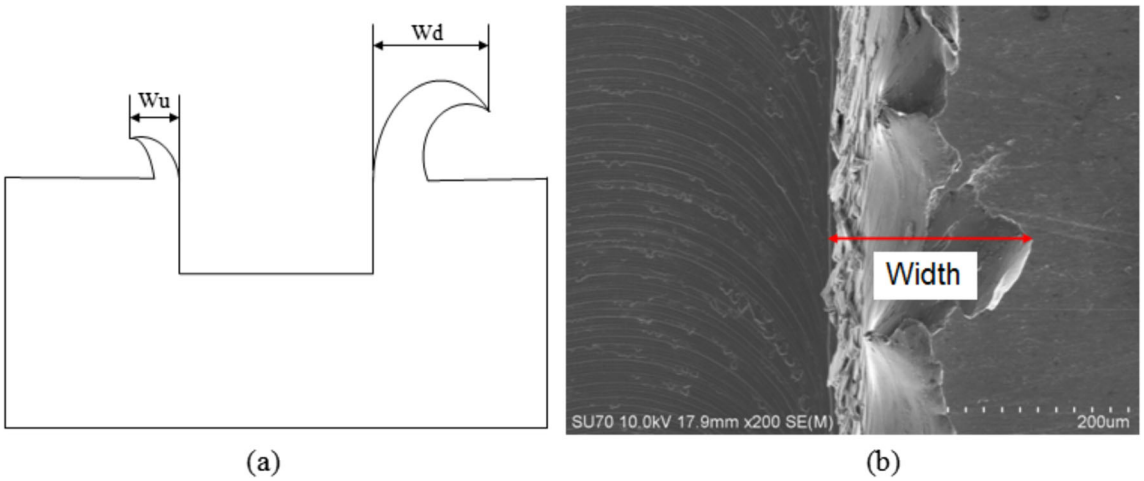


**Fig. 3** **a** Schematic of burr size on both up-milling and down-milling sides. **b** Measurement of burr width in SEM image

up-milling side), and exit burr. As shown in Fig. 5, entrance burr was generated on the down-milling side, and exit burr was generated on the up-milling side in general. The entrance burr was bigger than exit burr. Top burr occurred in two sides along the microchannels. The comparison of burr formation in the experiments by SEM images and FE simulation indicates that the simulation results were in fairly good agreement with experiment. As the top burrs played a major role on the microchannel surface qualities, the top burr formations were focused on in micro-milling of microchannels, which is similar to many other studies [13, 26, 27].

With the workpiece feeding movement and rotation of the cutter, the tool cut in from the up-milling side and cut out from the down-milling side. Different top burr formations occurred for the up-milling and down-milling side. On the up-milling side, when the materials were firstly cut by the tool, the uncut chip thickness increased from zero to a maximum large value at approximately the center of the channel [28]. The material was plowed, squeezed, and elastically recovered with no chips (Fig. 6(a1)) in the early stage of each tool rotation cycle, as the instantaneous uncut chip thickness was less than the minimum chip thickness. With the rotation and feeding movement of the tool, the shearing process turns to dominate in the middle and last stage of each tool rotation cycle on the up-milling side, as the uncut chip thickness began to exceed the minimum chip thickness. Most part of materials teared under large tensile stress and formed small chips (Fig. 6(a2)), and some part of materials near the end of workpiece were not taken away with the chip due to the lack of enough tool-chip engagement. They stay along the top of microchannel walls and formed the initial small top burrs (Fig. 6(a3)). During the following tool pass cycles, these initial top burrs were pushed outwards slightly by the cutting tool edge under the combined effects of plowing and extrusion [29], and the small top burrs in the on the up-milling side were finally formed (Fig. 6(a4)).

On the other hand, when the edge of cutter was rotated further to the down-milling side after the tool crossed the center of the channel, the work piece materials were compressed and bulged to the down-milling side along the rake face (Fig. 6(b1)). The uncut chip thickness decreased from a

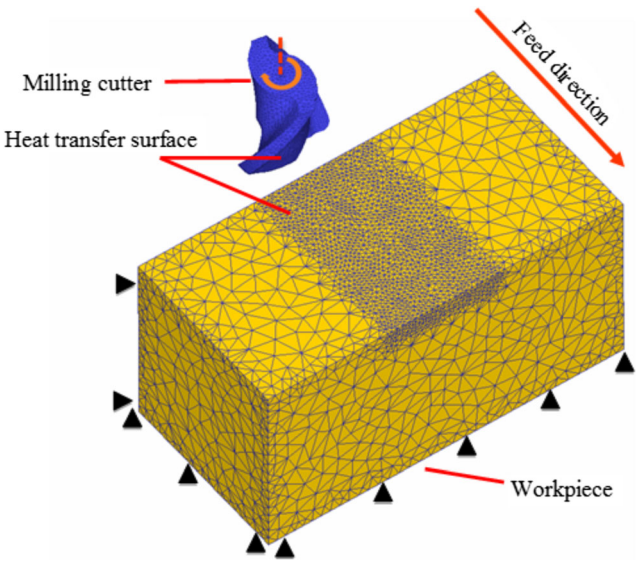


**Fig. 4** Geometry and mesh models in the simulation

**Table 3** Physical properties of copper

| Parameter | Value |
|---|---|
| Density, $\rho$ (kg/m$^3$) | $8.96 \times 10^3$ |
| Young's modulus, $E$ (GPa) | 124 |
| Shear modulus (GPa) | 47.7 |
| Poisson's ratio, $\mu$ | 0.33 |
| Specific heat J/(kg °C) | 385 |
| Thermal conductivity W/(m °C) | 391 |

**Table 4** Parameters of the tungsten carbide micro-end mills

| Parameter | Value |
|---|---|
| Density, $\rho$ (kg/m$^3$) | $1.44 \times 10^4$ |
| Poisson's ratio, $\mu$ | 0.28 |
| Young's modulus, $E$ (GPa) | 540 |
| Bending strength (GPa) | 4.0 |

maximum large value to zero. Large plastic deformation occurred on the surface of materials. Some deformed materials were pushed outwards remarkably by the cutting edge until permanent plastic deformation occurred, and the chips separated from the workpiece base by tear separation (Fig. 6(b2)). Here, the instantaneous uncut chip thickness was larger than the minimum chip thickness. When the uncut chip thickness was decreased, the materials tended to be not clearly cut. They still stick to the workpiece due to a lack of sufficient tool-chip interaction, and extruded and rubbed further. They formed the initial top burrs on the down-milling side (Fig. 6(b3)). When the cutter continued to rotate to the sidewall of the down-milling side in the next pass cycles, the deformed materials tended to roll over and cover the top surface. The final top burrs in down-milling side were thus induced (Fig. 6(b4)).

### 3.1.2 Effect of spindle speed on burr size

Figure 7 shows the microscopic images of microchannels with top burrs in different spindle speeds. It is clear that the top burrs on the down-milling side were much larger and wider than that on the up-milling side. This can be linked to the aforementioned different burr formation process in both up-milling and down-milling sides. Ideally, the chips separated at the end of each cutter pass. This is true for the up-milling process, as the shearing process dominated with chip removement in the middle and last stage of each tool rotation cycle. Tiny and thin burrs formed on the up-milling side. On the contrary, for the down-milling process, friction and squeezing effect dominated between cutter and workpiece instead of shearing in the down-milling side, as the uncut chip thickness tended to decrease to be less than the minimum chip thickness in the middle and last stage of each tool rotation cycle. The deformed materials still stick to the workpiece due to a lack of sufficient tool-chip interaction, and were extruded and rubbed further. Some parts of materials flew along the cutter, and rolled over and covered the top surface. Thus, much larger top burrs can be formed on the down-milling side. This can be also noted in the figures of Fig. 8, Fig. 10, and Fig. 12. Such results have been also observed by Kiswanto et al. [13], Wu et al. [21], and Vipindas et al. [30].

When the spindle speed increased from 9000 to 21,000 r/min, the top burrs tended to weaken on the down-milling side, and the burr width on the down-milling side reduced remarkably, as shown in Fig. 8. This can be related to the fact that insufficient time were provided for plastic deformation when machining at high cutting speed. The friction between the workpiece and the tool was reduced considerably, and the cutting forces were thus reduced [31]. More stable micro-milling process was induced during the fabrication of micro-channels, and the deformed materials to form top burrs were decreased. Nevertheless, the top burr width on the up-milling side changed very slightly with the increasing cutting speed, as shown in Fig. 8. This suggests that the cutting speed played a negligible role on the top burr width on the up-milling side. In conclusion, in order to reduce the top burr formations in the micro-milling of microchannels, high spindle speed is favorable and should be chosen.

**Table 5** Parameter in J-C model

| J-C parameter | Value |
|---|---|
| $A$ (GPa) | 0.09 |
| $B$ (GPa) | 0.292 |
| $C$ | 0.025 |
| $n$ | 0.31 |
| $m$ | 1.09 |
| $T_{room}$ (K) | 293 |
| $T_{melt}$ (K) | 1356 |

### 3.1.3 Effect of feed rate on burr size

Figure 9 shows the top burr morphologies on microchannels micro-milled in different feed rates. When the smallest feed rate of 30 mm/min was imposed, which corresponded to 1 μm per tooth (1 μm/z), notable top burrs can be found on the down-milling side of microchannels. When the feed rate increased from 30 mm/min (1 μm/z) to 60 mm/min (2 μm/z), the top burrs tended to reduce considerably, and the top burr width decreased remarkably, as shown in Fig. 10. When the feed rate increased from 90 mm/min (3 μm/z) to 150 mm/min (5 μm/z), the top burr width increases notably. The above trend of top burr size may be due to that the feed rate ($f_z$) of 2 μm/z is equal to the value of tool cutting edge radius ($r_e$), and different burr formation processes occurred beyond this threshold value. In micro-milling, due to the size effect, when the feed rate per tooth was smaller than the tool cutting edge radius, negative rake angle was induced, and the plowing and extruding effect with elastic recovery played the dominating role on the material deformation instead of shearing and cutting off [17, 28]. The deformed materials were pushed upwards by the cutting edge, and the previously generated small burrs were scratched and accumulated to form relatively large rolling over top burrs [29]. Thus top burrs with large burr width occurred for the feed rate case of 30 mm/min (1 μm/z). The plowing and extruding effect tended to degrade when

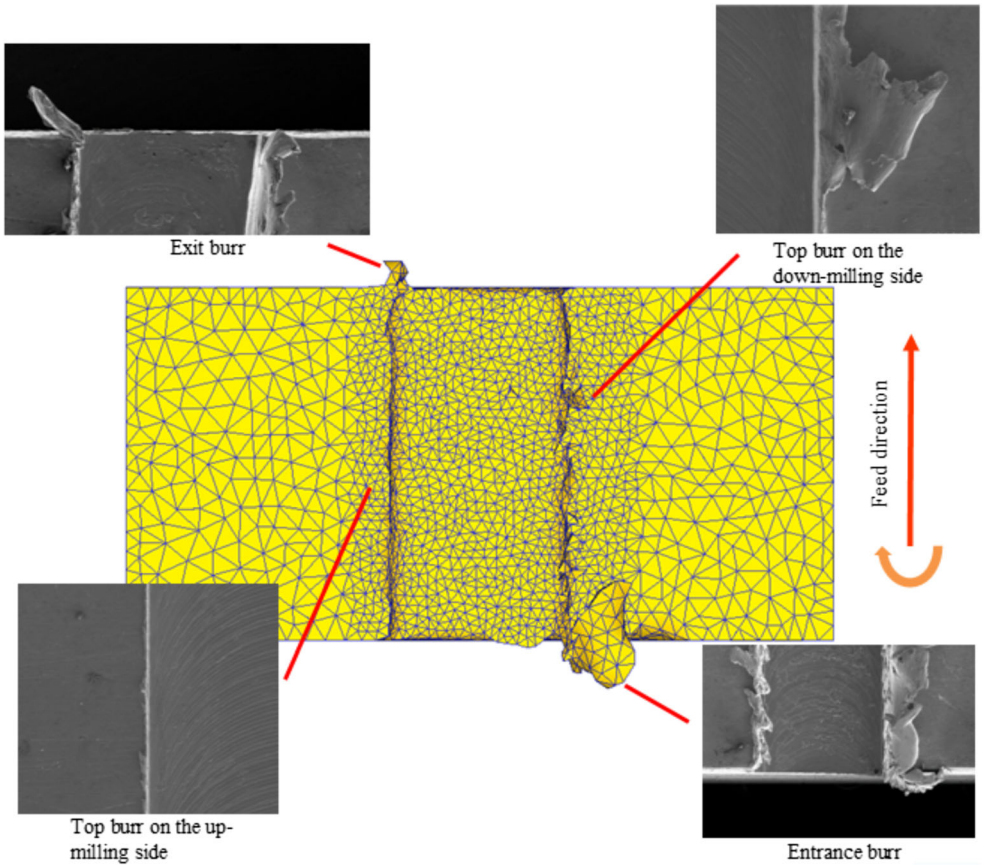


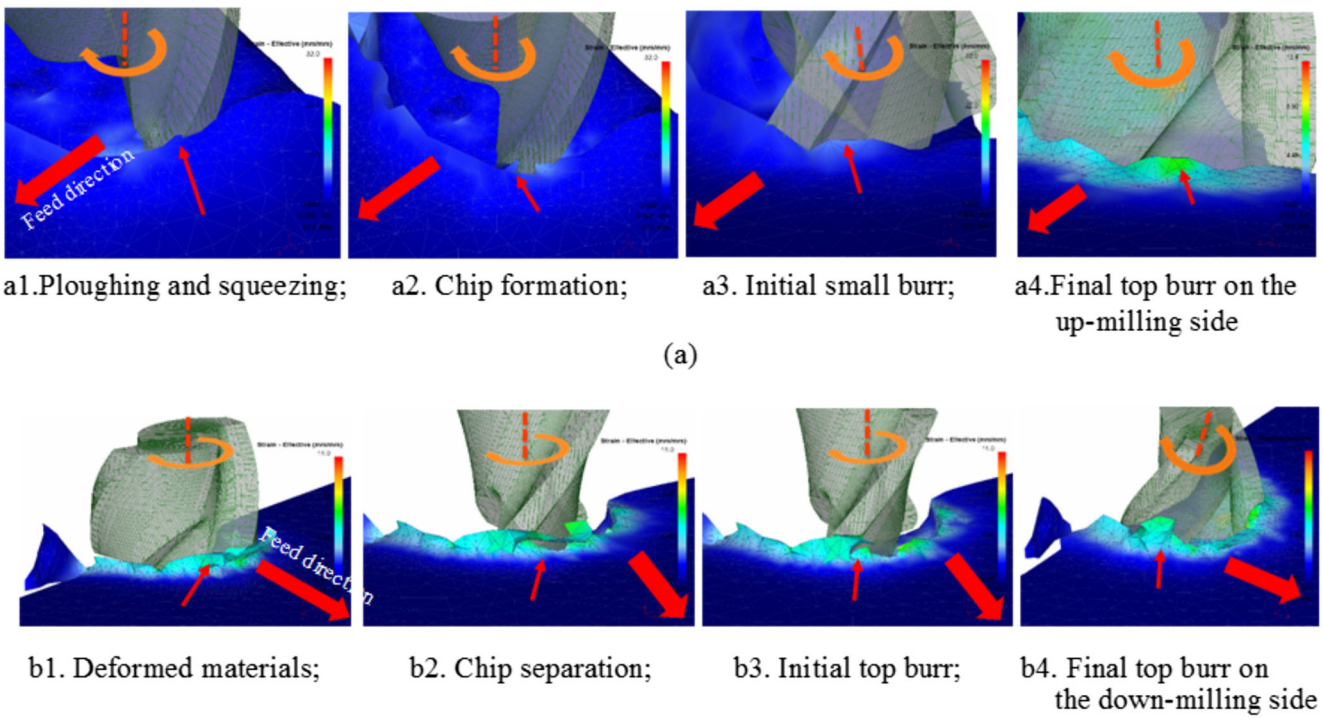


**Fig. 5** Burr formation in FE simulation and experiment observations by SEM

**Fig. 6** The top burr formation process. **a** Top burr formation process on the up-milling side. **b** Top burr formation process on the down-milling side

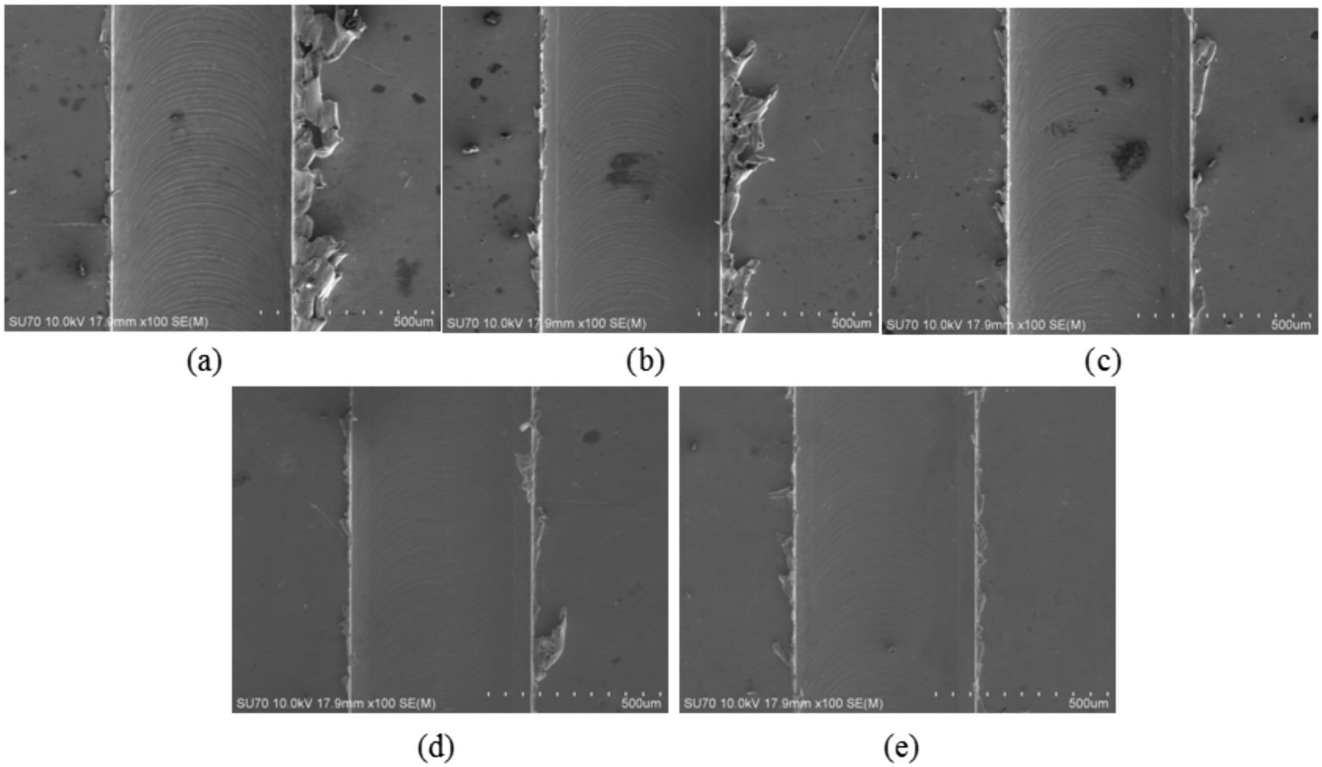


**Fig. 7** SEM images of burr formation of microchannels fabricated in different spindle speeds. **a** 9000 r/min. **b** 12,000 r/min. **c** 15,000 r/min. **d** 18,000 r/min. **e** 21,000 r/min

the feed rate approached to be the value of tool cutting edge radius, and the top burrs presented a reduction in their width. Nevertheless, when the feed rate exceeded the tool cutting edge radius, the shearing and cutting process became the dominant one during the micro-milling. With the feed rate increasing, the deformed materials increased by the intensification of rubbing and bulging. The chip became much thicker and larger top burrs were generated. Thus, the top burr size increased. From Fig. 10, it can be also noted the top burr width on the up-milling side maintained to be almost constant regardless of the increase in feed rate. From the above, it seems that the optimum feed rate is 60 mm/min (2 μm/z), which produced the smallest top burr width.

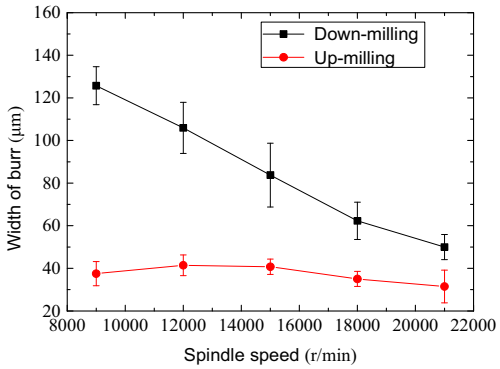


**Fig. 8** Top burr width of microchannels micro-milled in different spindle speeds

#### 3.1.4 Effects of depth of cut on burr size

The top burr morphologies on microchannels micro-milled in different depths of cut are shown in Fig. 11. Tiny top burrs were found when small depths of cut of less than 80 μm were employed, whereas remarkable top burrs occurred when the depths of cut increased to 80 μm and larger ones. The top burr size of the microchannels increased monotonically for both down-milling and up-milling side when the depth of cut was augmented, as shown in Fig. 12. This is consistent to the results of micro-ball end milling operation on Ti–6Al–4V by Chen et al. [29]. With the increase in depth of cut, the contact area between the tool and workpiece increased, and the extruding and scratching process were enlarged. The cutting force increases and the maximum effective strain are gradually increased [32]. Therefore, more material deformation was induced, and larger top burrs were formed along the cutting edge of tool. It suggests that small depth of cut can be adopted to reduce the formation of top burrs.

### 3.2 Surface roughness

#### 3.2.1 Effects of spindle speed on surface roughness

The surface profiles of the microchannel samples micro-milled in different spindle speeds are shown in Fig. 13.

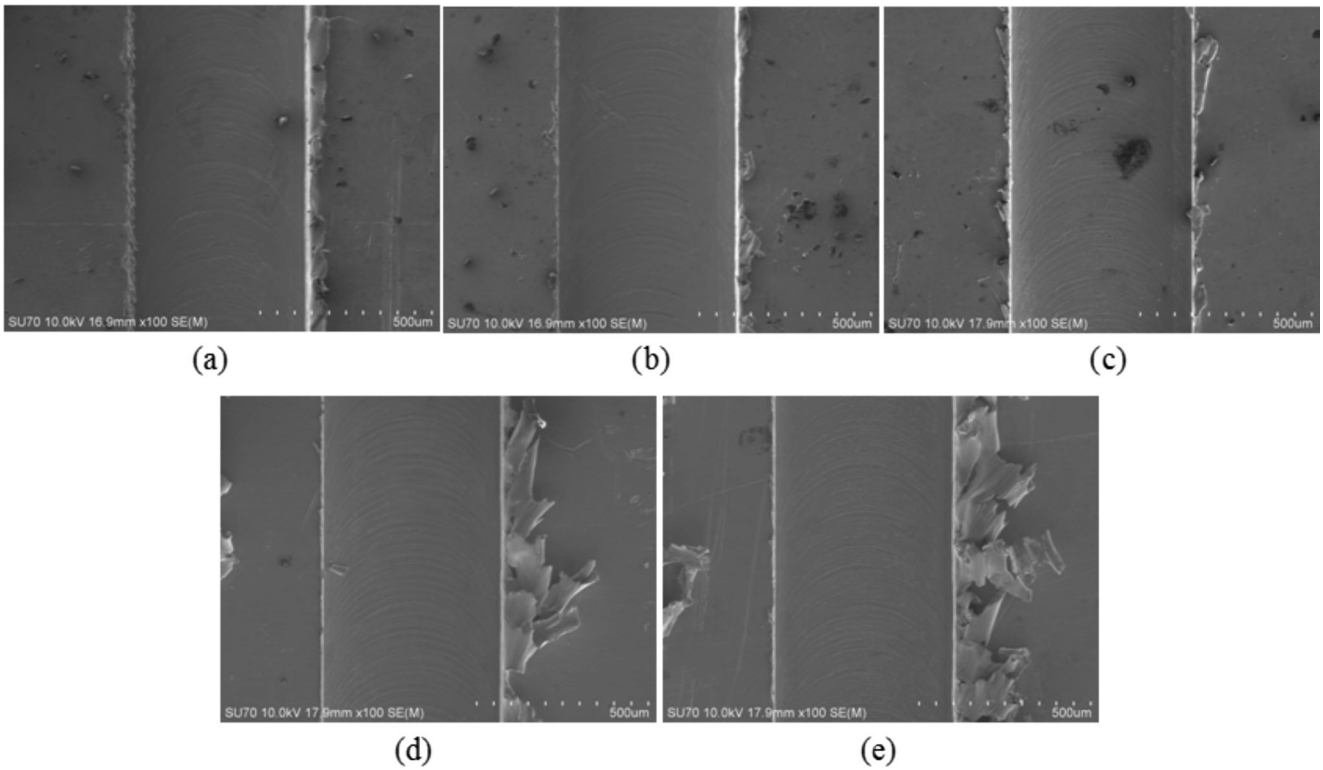


**Fig. 9** SEM images of burr formation of microchannels fabricated in different feed rates. **a** 30 mm/min. **b** 60 mm/min. **c** 90 mm/min. **d** 120 mm/min. **e** 150 mm/min

Figure 14 shows the surface roughness (Ra) of the microchannel bottom and two sidewalls. All the surface roughness of microchannel walls showed a monotonic decline with increasing spindle speed. Figure 15 illustrates the bottom surface images of microchannels with a low and high spindle speed of 9000 r/min and 21,000 r/min, respectively. It is clear that the high spindle speed case induced much less shallow scratches and more smooth surface on microchannel wall. As mentioned before, higher cutting speed contributed to a reduction of the contact time between the cutting edge of tool and the workpiece. The friction resistance between the tool rake face and metal scraps were reduced, and the cutting forces are reduced considerably. Therefore, the bending of tool was weakened, and the vibration during the micro-milling process was decreased. Therefore, better surface qualities of microchannels after micro-milling were induced with increasing cutting speed. Besides, it can be noted that rougher surfaces on the down-milling sidewall were obtained than that on the up-milling sidewall. Figure 16 illustrates the surface images of both up-milling and down-milling side of microchannels. It is clear that the down-milling sidewall surface featured wave-shaped scratches, whereas the up-milling sidewall surface was relatively smooth. As mentioned in Section 3.1.1, on the down-milling process, the uncut chip thickness decreased from large values to zero. It was firstly larger than the minimum chip thickness, and then tended to be equal or less than the minimum chip thickness with the tool rotation. The shearing effect was thus decreased, and the unremoved materials were extruded and rubbed by the cutter. Under the combined effects of squeezing, friction, and heat accumulation, a small part of materials on down-milling side melt. Some deformed materials still stick to the down-milling sidewall and elastic recovery occurred, forming a rough surface with wave-shaped scratches, as shown in Fig. 16a. On the other side, for the up-milling process, the uncut chip thickness

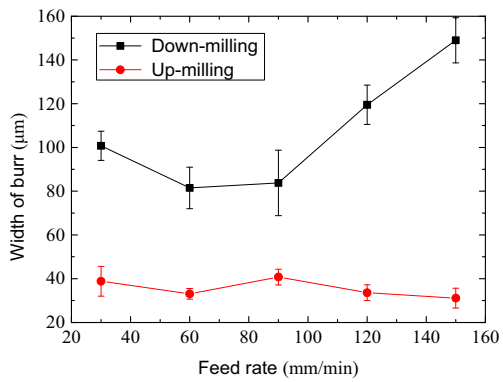


**Fig. 10** Top burr width of microchannels micro-milled in different feed rates

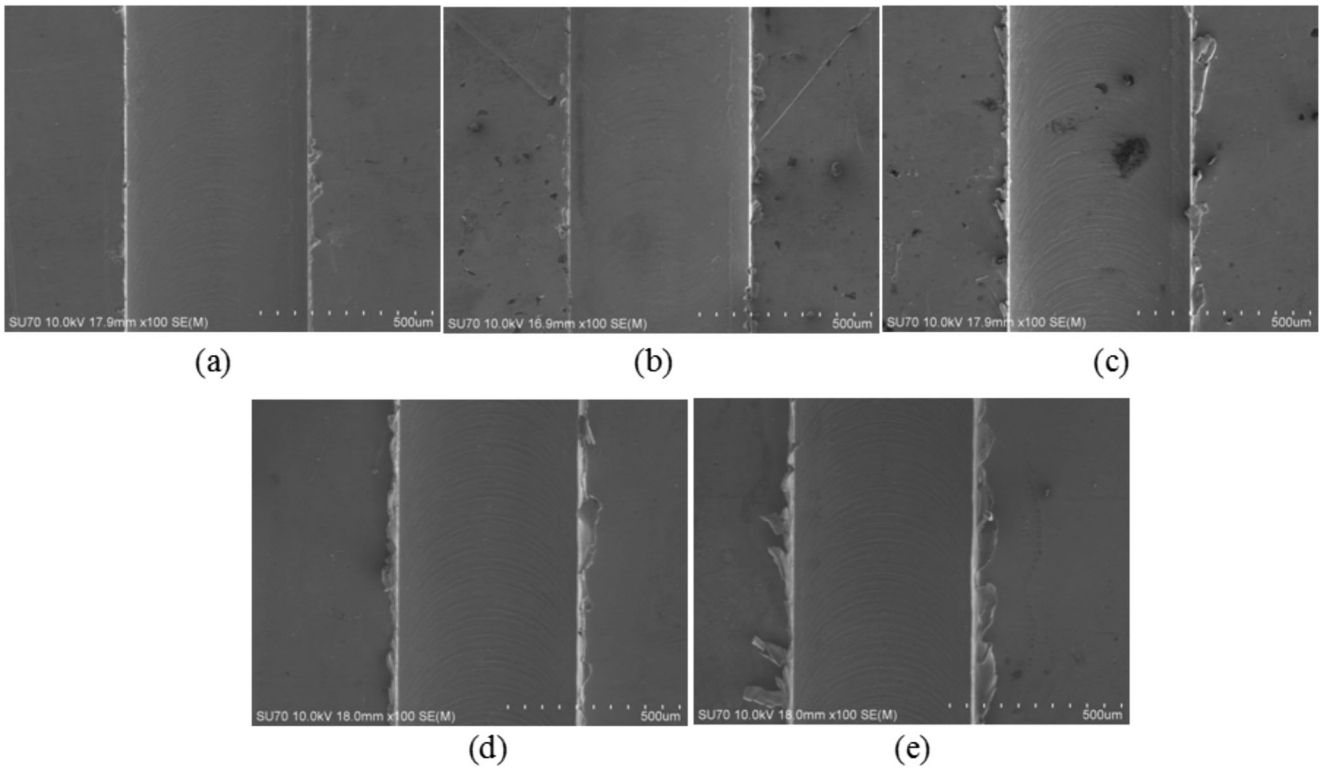


**Fig. 11** SEM images of burr formation of microchannels fabricated in different depths of cut. **a** 40 μm. **b** 60 μm. **c** 80 μm. **d** 100 μm. **e** 120 μm

increased to be large values and exceed the minimum chip thickness with the rotation and feeding movement of the tool. The shearing effect dominated in the middle and last stage of up-milling process, and the chip can be removed continuously. Thus, fairly smooth surfaces can be obtained on the up-milling side.

### 3.2.2 Effects of feed rate on surface roughness

Figure 17 shows surface profiles of the microchannel samples fabricated in different feed rates. The surface roughness (Ra) of the microchannel bottom and two sidewalls micro-milled are given in Fig. 18. The down-milling sidewall presented the largest surface roughness, followed by the up-milling sidewall. The bottom surface of microchannels showed the smallest surface roughness with more smooth surfaces. It can be found that the Ra of microchannel walls presented non monotonic tendencies, i.e., it firstly decreased and reached the minimum, and then changed to ascend with increasing feed rates. As aforementioned in Section 3.1.3, when the feed rate increased from 30 mm/min (1 μm/z) to 60 mm/min (2 μm/z) and 90 mm/min (3 μm/z), the feed rate is firstly smaller than the value of the tool cutting edge radius, and then tended to be equal to or slightly larger than tool cutting edge radius. The effective rake angle at the cutting edge was negative. The plowing and extruding effect with elastic recovery instead of the shearing dominates during the micro-milling process, which played a negative effect on the roughness. Therefore, an early decrease in the roughness can be noted. After 60 mm/min (2 μm/z) and 90 mm/min (3 μm/z) feed, the roughness began to increase with the increasing in feed rate. In these conditions, the feed rate exceed the tool cutting edge radius, and the shearing and cutting process became more dominant. It contributed to more plastic deformation, and induced more rubbing and bulging. Rougher microchannel wall surfaces were obtained. The above tendency of surface roughness was consistent in other studies of micro-milling [33, 34]. From the above, it can be noted a moderate feed rate close to

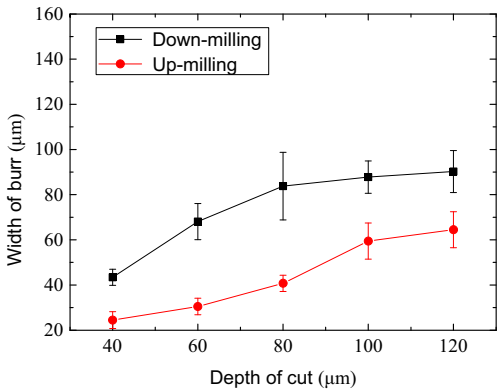


**Fig. 12** Top burr width of microchannels micro-milled different depths of cut

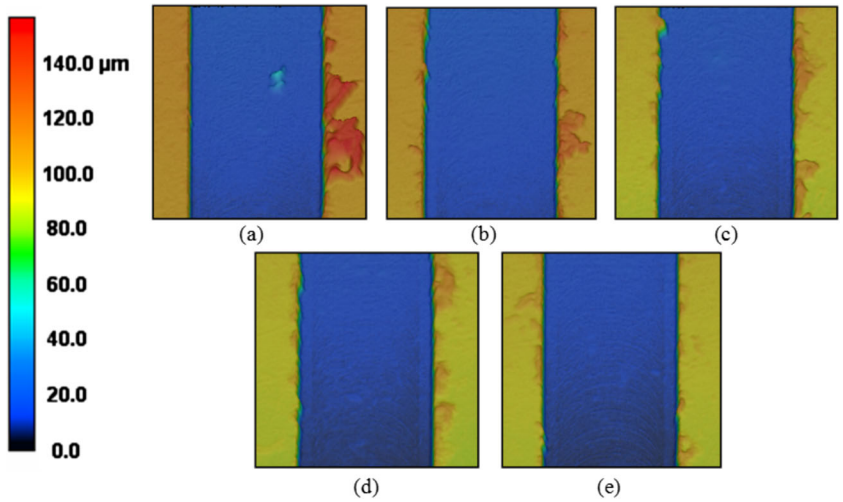


**Fig. 13** Profile images of micro-channels micro-milled in different spindle speeds. **a** 9000 r/min. **b** 12,000 r/min. **c** 15,000 r/min. **d** 18,000 r/min. **e** 21,000 r/min

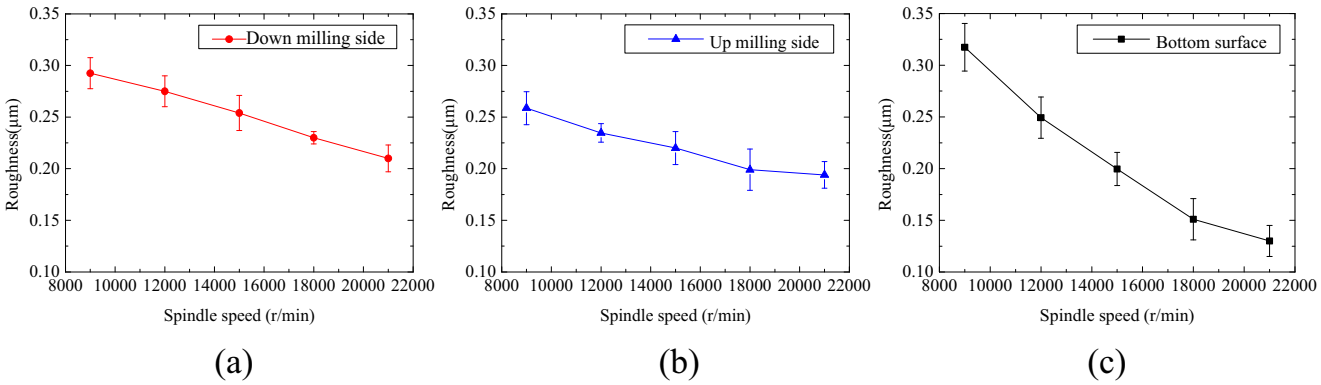


**Fig. 14** Surface roughness of microchannel walls as a function of spindle speed. **a** Down-milling side. **b** Up-milling side. **c** Bottom wall

the tool cutting edge radius should be selected with improved surface finish of microchannels.

### 3.2.3 Effects of depth of cut on surface roughness

Figure 19 shows surface profiles of the microchannel samples fabricated in different depths of cut. The surface roughness of the bottom and both sidewall of microchannels are shown in Fig. 20. A monotonic increase in Ra can be noted with the increasing the depth of cut. When the depth of cut increased from 40 to 120 μm, the volume of chip removal per unit time was increased as the feed rate and the spindle speed were consistent. This increased the cutting force when the tool contacted with the workpiece. More vibration and bending

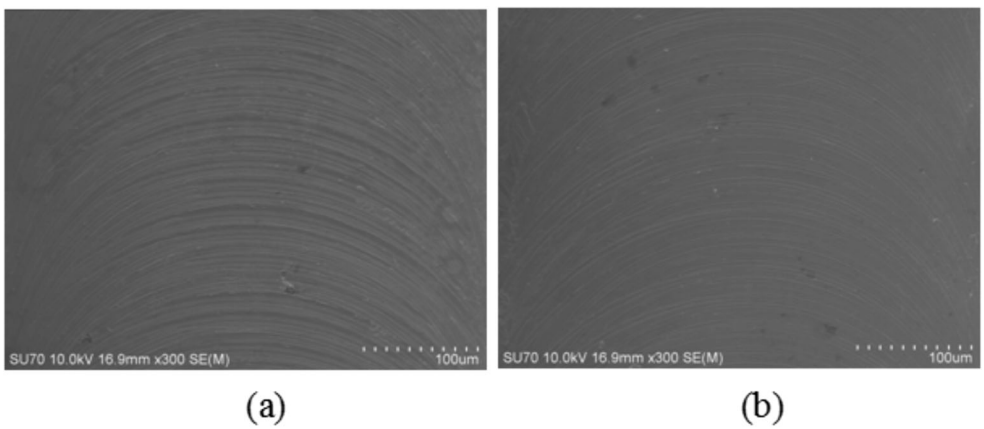


**Fig. 15** SEM images of bottom wall surface of microchannels under different spindle speeds. **a** 9000 r/min. **b** 21,000 r/min

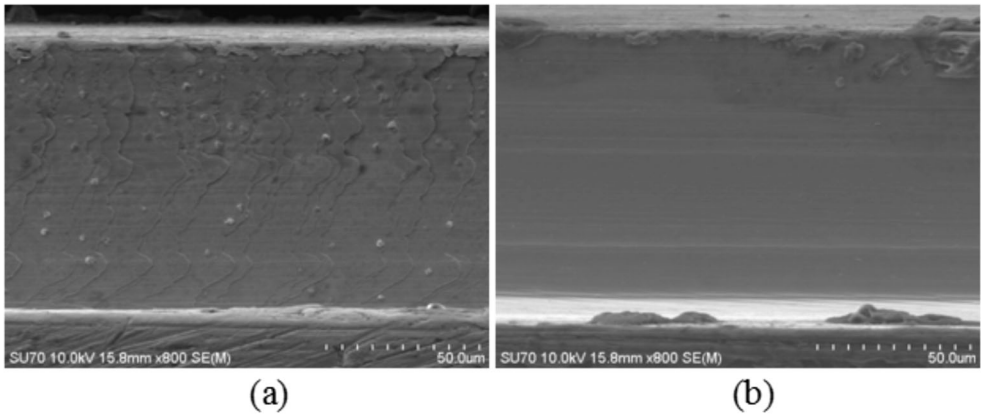


**Fig. 16** SEM images of sidewall surface under the same spindle speed of 12,000 r/min. **a** Down-milling side. **b** Up-milling side

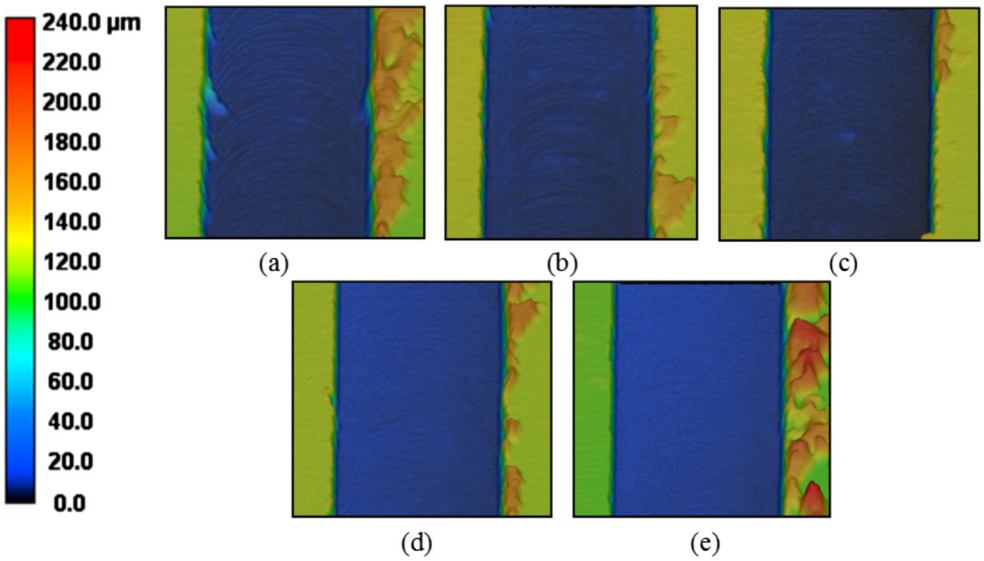


**Fig. 17** Profile images of micro-channels micro-milled in different feed rates. **a** 30 mm/min. **b** 60 mm/min. **c** 90 mm/min. **d** 120 mm/min. **e** 150 mm/min

deformation of the tool were induced as the stiffness of tool was constant. Therefore, more scratches were induced, and rougher microchannel wall surfaces were induced. Therefore, improved surface finish can be obtained by smaller depth of cut.

## 4 Conclusion

In this study, copper microchannels were fabricated by a micro-milling process. The burr formation and surface roughness of microchannel bottom and sidewalls were investigated

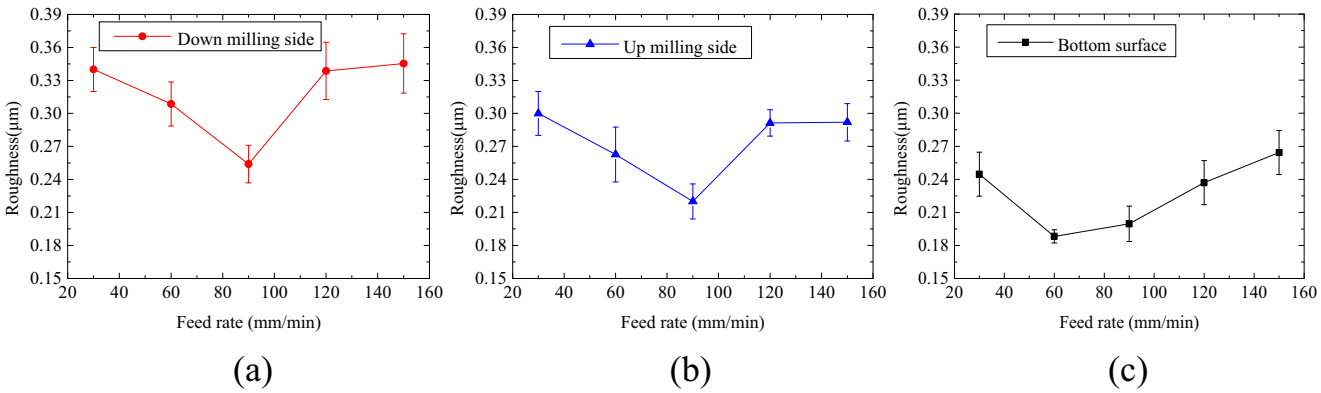


**Fig. 18** Surface roughness of microchannel walls as a function of feed rate. **a** Down-milling side. **b** Up-milling side. **c** Bottom surface

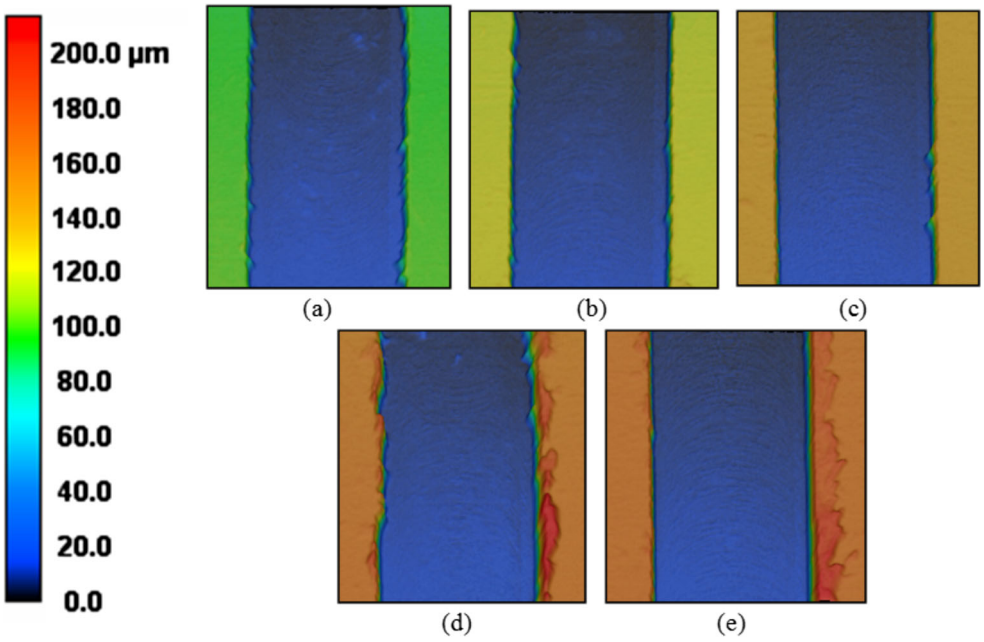


**Fig. 19** Profile images of micro-channels micro-milled in different depths of cut. **a** 30 mm/min. **b** 60 mm/min. **c** 90 mm/min. **d** 120 mm/min. **e** 150 mm/min

in the micro-milling process of microchannels. The formation mechanism of burrs along the microchannels was studied via 3D finite element simulation together with experiment observations. Various micro-milling processing parameters, including spindle speed, feed rate, and depth of cut, were investigated by experiment, particularly on their effects on surface roughness and burr formation of microchannels. Main conclusions were summarized as follows:

(1) Top burr formation and its size on the down-milling side were much larger than those on the up-milling side in the micro-milling of microchannels.

(2) Top burr formations and its size on the down-milling side of microchannels decreased monotonically when the spindle speed increased, whereas it presented an opposite increasing trend with larger depth of cut. The top burrs on the up-milling side of microchannels maintained to be almost unchanged with the variation of spindle speed and feed rate, but they tend to increase with increasing depth of cut.

(3) When the feed rate increased from 30 mm/min (1 μm/z) to 150 mm/min (5 μm/z), the top burr size on the down-milling side of microchannels firstly decreased, and then tended to increase. This phenomenon can be related to that the plowing and extruding effect together with elastic recovery played the dominating role on the material deformation when the feed rate per tooth was smaller than the tool cutting edge radius, whereas the shearing and cutting process turn to dominate after the feed rate per tooth exceeds the tool cutting edge radius.

(4) The variations of surface roughness of microchannel bottom and both sidewalls were generally in line with the top burr size on the down-milling side when the above micro-milling parameters changed.

(5) In order to improve the surface quality of micro-channels, high spindle speed, small depth of cut, and the

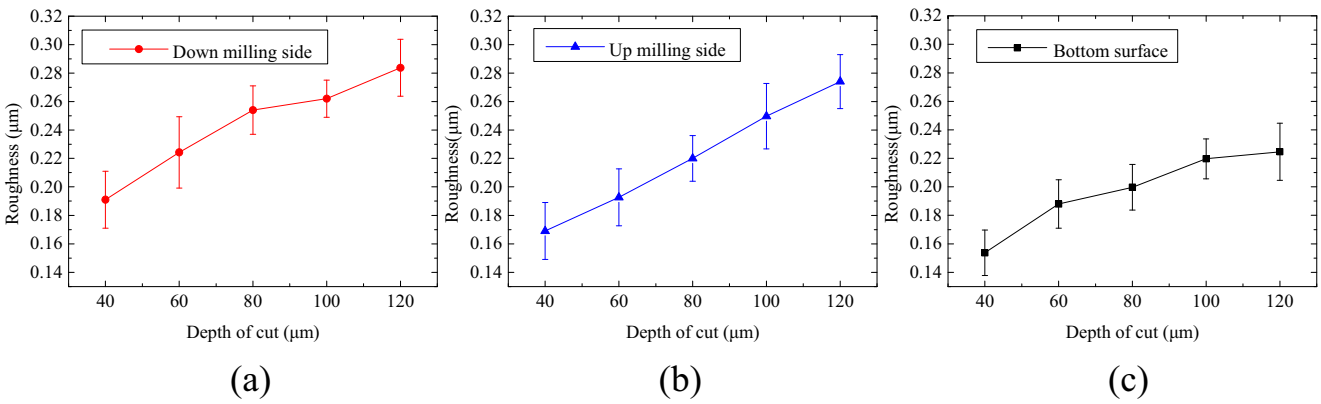


**Fig. 20** Surface roughness of microchannel walls as a function of depth of cut. **a** Down-milling side. **b** Up-milling side. **c** Bottom surface

moderate feed rate close to the tool cutting edge radius should be selected for the optimum.

**Acknowledgments** This study was financially supported under the Grants of the National Nature Science Foundation of China (No. 51775464), and is partially supported by Natural Scientific Research Innovation Foundation in Harbin Institute of Technology (Project HIT.NSRIF.2020067). We also would like to thank Mr. Wei Wan for his help in the experiments.

## References

1. Deng D, Wan W, Qin Y, Zhang J, Chu X (2017) Flow boiling enhancement of structured microchannels with micro pin fins. Int J Heat Mass Transfer 105:338–349
2. Deng D, Wan W, Tang Y, Wan Z,Liang D (2015)Experimental investigations on flow boiling performance of reentrant and rectangular microchannels – a comparative study. Int J Heat Mass Transf 82:435–446
3. Tuckerman DB, Pease RFW (1981) High-performance heat sinking for VlSI. IEEE Electron Device Letter 5:126–129
4. Silvério V, Cardoso S, Gaspar J, Freitas PP, Moreira ALN (2015) Design, fabrication and test of an integrated multi-microchannel heat sink for electronics cooling. Sensor Actuat A: Phys 235:14–27
5. Wang GJ, Hsueh CC, Hsu SH, Hung HS (2007) Fabrication of PLGA microvessel scaffolds with circular microchannels using soft lithography. J Micromech Microeng 17:2000–2005
6. Chu X, Zeng X, Zhuang W, Zhou W, Quan X, Fu T (2019) Vibration assisted high-speed wire electric discharge machining for machining surface microgrooves. J Manuf Process 44:418–426
7. Deng D, Xie Y, Chen L, Chen X (2019) Experimental investigation on laser micromilling of SiC microchannels. Int J Adv Manuf Technol 101:9–21
8. Prakash S, Kumar S (2014) Fabrication of microchannels: a review. Proc Inst Mech Eng Pt B: J Eng Manuf 229:1273–1288
9. Wan Z, Li Y, Tang H, Deng W, Tang Y (2014) Characteristics and mechanism of top burr formation in slotting microchannels using arrayed thin slotting cutters. Precis Eng 38:28–35
10. Gao P, Wang X, Liang Z, Xiang J, Li W, Xie J (2019) Effects of WC grain size and Co content on microscale wear behavior of micro end mills in aluminum alloy 7075 machining. Int J Adv Manuf Technol 104:2401–2413
11. Vázquez E, Rodríguez CA, Elías-Zúñiga A, Ciurana J (2010) An experimental analysis of process parameters to manufacture metallic micro-channels by micro-milling. Int J Adv Manuf Technol 51:945–955
12. Vázquez E, Ciurana J, Rodríguez CA, Thepsonthi T, Özel T (2011) Swarm intelligent selection and optimization of machining system parameters for microchannel fabrication in medical devices. Mater Manuf Process 26:403–414
13. Kiswanto G, Zariatin DL, Ko TJ (2014) The effect of spindle speed, feed-rate and machining time to the surface roughness and burr formation of Aluminum Alloy 1100 in micro-milling operation. J Manuf Process 16:435–450
14. Wang Y, Zou B, Huang C, Liu Z, Yao P (2018) The micro-cutting performance of cermet and coated WC micro-mills in machining of TC4 alloy micro-grooves. Int J Adv Manuf Technol 96:1403–1414
15. Han J, Hao X, Li L, Liu L, Chen N, Zhao G, He N (2020) Investigation on surface quality and burr generation of high aspect ratio (HAR) micro-milled grooves. J Manuf Process 52:35–43
16. Wang W, Kweon SH, Yang SH (2005) A study on roughness of the micro-end-milled surface produced by a miniatured machine tool. J Mater Process Tech 162-163:702–708
17. Jin CZ, Kang IS, Park JH, Jang SH, Kim JS (2009) The characteristics of cutting forces in the micro-milling of AISI D2 steel. J Mech Sci Technol 23:2823–2829
18. Biermann D, Kahnis P (2009) Analysis and simulation of size effects in micromilling. Production Eng 4:25–34
19. Özel T, Thepsonthi T, Ulutan D, Kaftanoğlu B (2011) Experiments and finite element simulations on micro-milling of Ti–6Al–4V alloy with uncoated and cBN coated micro-tools. CIRP Ann 60:85–88
20. Lekkala R, Bajpai V, Singh RK, Joshi SS (2011) Characterization and modeling of burr formation in micro-end milling. Precis Eng 35:625–637
21. Wu X, Li L, He N (2017) Investigation on the burr formation mechanism in micro cutting. Precis Eng 47:191–196
22. Gao Q, Gong Y, Zhou Y, Wen X (2017) Experimental study of micro-milling mechanism and surface quality of a nickel-based single crystal superalloy. J Mech Sci Technol 31:171–180
23. Piquard R, D'Acunto A, Laheurte P, Dudzinski D (2014) Micro-end milling of NiTi biomedical alloys, burr formation and phase transformation. Precis Eng 38:356–364
24. Wu X, Li L, He N, Zhao M, Zhan Z (2015) Investigation on the influence of material microstructure on cutting force and bur formation in the micro cutting of copper. Int J Adv Manuf Technol 79: 321–327
25. Johnson GR, Cook WH (1983) A constitutive model and data for metals subjected to large strains, high strain rates and high temperature. Proceedings of the Seventh International Symposium on Ballistics. The Haque, The Netherlands
26. Hassanpour H, Sadeghi MH, Rezaei H, Rasti A (2016) Experimental study of cutting force, microhardness, surface roughness, and burr size on micromilling of Ti6Al4V in minimum quantity lubrication. Mater Manuf Process 31:1654–1662
27. Zhao K, Jia Z, Liu W, Ma J, Ding L (2015) Burr control for removal of metal coating from plastics substrate by micro-milling. Mater Manuf Process 31:641–647
28. Filiz S, Conley CM, Wasserman MB, Ozdoganlar OB (2007) An experimental investigation of micro-machinability of copper 101 using tungsten carbide micro-endmills. Int J Mach Tools Manuf 47:1088–1100
29. Chen MJ, Ni HB, Wang ZJ, Jiang Y (2012) Research on the modeling of burr formation process in micro-ball end milling operation on Ti–6Al–4V. Int J Adv Manuf Technol 62:901–912
30. Vipindas K, Kuriachen B, Mathew J (2016) Investigations into the effect of process parameters on surface roughness and burr formation during micro end milling of TI-6AL-4V. Int J Adv Manuf Technol 100:1207–1222
31. Afazov SM, Ratchev SM, Segal J (2010) Modelling and simulation of micro-milling cutting forces. J Mater Process Tech. 210:2154–2162
32. Yang K, Bai QS, Yu FL, Liang YC (2010) Modelling and experimental analysis of the mechanism of micro-burr formation in micro-end-milling process. Nano Precis Eng 8:75–83
33. Aramcharoen A, Mativenga PT (2009) Size effect and tool geometry in micromilling of tool steel. Precis Eng 33:402–407
34. Huo D, Cheng K (2010) Experimental investigation on micromilling of oxygen-free, high-conductivity copper using tungsten carbide, chemistry vapour deposition, and single-crystal diamond micro tools. Proc Inst Mech Eng Pt B: J Eng Manuf. 224: 995–1003